HITLESS MEMORY-RECONFIGURABLE PHOTONIC RESERVOIR COMPUTING ARCHITECTURE

A PREPRINT

Mohab Abdalla[1,2], **Clément Zrounba**[1], **Raphael Cardoso**[1], **Paul Jimenez**[1], **Guanghui Ren**[2], **Andreas Boes**[2], **Arnan Mitchell**[2], **Alberto Bosio**[1], **Ian O'Connor**[1], **Fabio Pavanello**[1]

[1]Univ. Lyon, Ecole Centrale de Lyon, INSA Lyon, UCB Lyon, CPE Lyon, CNRS, Lyon Institute of Nanotechnology

[2]School of Engineering, RMIT University

ABSTRACT

Reservoir computing is an analog bio-inspired computation model for efficiently processing time-dependent signals, the photonic implementations of which promise a combination of massive parallel information processing, low power consumption, and high speed operation. However, most implementations, especially for the case of time-delay reservoir computing (TDRC), require signal attenuation in the reservoir to achieve the desired system dynamics for a specific task, often resulting in large amounts of power being coupled outside of the system. We propose a novel TDRC architecture based on an asymmetric Mach-Zehnder interferometer (MZI) integrated in a resonant cavity which allows the memory capacity of the system to be tuned without the need for an optical attenuator block. Furthermore, this can be leveraged to find the optimal value for the specific components of the total memory capacity metric. We demonstrate this approach on the temporal bitwise XOR task and conclude that this way of memory capacity reconfiguration allows optimal performance to be achieved for memory-specific tasks.

Keywords Reservoir Computing · Memory Capacity · Integrated Photonics

1 Introduction

The rising amount of data generated by our increasingly connected society calls for a paradigm shift in information processing. This need has sparked a strong interest in the community for alternative methods beyond classical Von-Neumann architectures, which suffer from the memory-to-processor communication bottleneck. Much interest is currently directed towards neuromorphic computing paradigms, which are essentially machine learning frameworks for performing computation in an intertwined, brain-inspired manner, not limited by the transfer of information from memory to processor. Reservoir computing (RC) is one type of neuromorphic computing which has garnered widespread interest since it was conceived by Jaeger [1] and Maas et al. [2] thanks to a simplified training phase when compared

to other recurrent neural network (RNN) approaches. RC architectures consist of 3 layers as shown in Fig. 1: an input layer where data is injected and/or pre-processed, a reservoir layer where the input signal is used to drive the dynamical nodes, and finally the output layer where the response of the reservoir is captured and trained for the desired tasks.

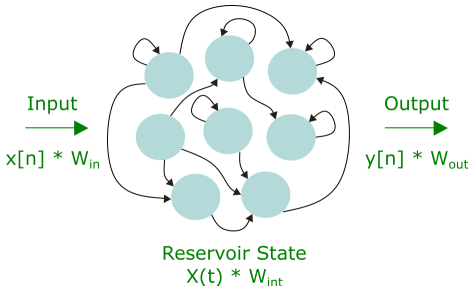

Fig. 1: Abstract representation of a reservoir computer.

RC is essentially a simplified recurrent neural network where only the output layer weights need to be trained, and the input and internal weights are set and fixed to values that depend on the desired dynamical regime for a given training task. The main idea lies in projecting the input data onto a higher dimensional state-space such that it becomes easier to find planes that linearly separate the different classes of data. Training the output layer can thus be done with simpler learning algorithms such as regression. Consequently, it has thus far enjoyed a multitude of hardware demonstrations across many technologies and platforms [3], especially in photonics using bulk optics [4, 5, 6], and, more recently, on photonic integrated circuits (PICs) [7, 8, 9]. A particular surge in PIC implementations is in large part due to their improved performance compared to electronic approaches in terms of power consumption, speed, footprint, and cost [7].

Time-delay reservoir computing (TDRC), first introduced in 2011 [10], offers a footprint-friendly solution for hardware implementations, requiring only a single physical node connected to itself with a delay line. The delay line is sampled N times in the span of one input bit, such that the N samples obtained can be viewed as the responses of N equidistant "virtual" nodes of the reservoir. A prediction is made by the weighted linear combination of the output response every N samples.

The linear memory capacity is one of the fundamental tasks for reservoir computing, which aims to test the echo state property by training the reservoir to reconstruct an input stream of values [0,1) drawn from an independent and identical distribution (i.i.d.) k timesteps later. It was first introduced in [11] and is given by:

$$MC = \sum_{k=1}^{N} MC_k \tag{1}$$

$$MC_k = \frac{cov(u(t-k), y_k(t))^2}{var(u(t))var(y_k(n))} = 1 - NMSE \tag{2}$$

$$NMSE = \frac{\langle \|y(n) - y_{exp}(n)\|^2 \rangle}{\langle \|(y_{exp}(n)) - \langle y_{exp}(n) \rangle\|^2 \rangle} \tag{3}$$

where N is the number of nodes, $NMSE$ is the normalized mean square error, $u(t)$ is the input, y_{exp} is the expected value, and MC_k [0,1] is the memory capacity for a k bits shift, which has been proven to be the theoretical upper limit for the summation in the same work [11]. $MC_k = 1$ corresponds to a perfect recall of the bitstream k bits later, while $MC_k = 0$ corresponds to the opposite.

While some theoretical studies have shed some light onto how to optimize the total memory capacity of a system [12, 13, 14], optimizing for a specific MC_k remains understudied in the literature, even though it may be important to consider, especially for applications that may require only the recall of specific k inputs into the past. It is generally assumed that a system with a given linear memory capacity can handle tasks requiring that memory capacity or less, without considering the specific memory capacity values associated with every k, which may need to be optimized.
In this work, we propose a novel photonic architecture based on an asymmetric MZI for TDRC and suggest coupling modulation [15] as a means of varying the memory capacity of the system without losing optical power in the process, in contrast to more common approaches relying on an attenuator block in the feedback loop. We leverage this architecture to investigate the effect of optimizing the individual components of the memory capacity metric and whether it is relevant for other memory-specific tasks, such as the temporal bitwise XOR.

2 Reservoir Architecture

The all-optical reservoir is based on an asymmetric MZI used in a feedback configuration by means of a delay line. The asymmetric MZI is based on two 3dB directional couplers with different arm lengths (1.5 mm and 3.0 mm) in between, as shown in Fig. 2. The top ports of the MZI are connected to each other by a spiral waveguide of length 4.15 cm, which constitutes the delay line. This architecture resembles an all-pass ring resonator, although the asymmetric MZI leads to an additional wavelength selectivity arising from the difference in arm lengths. In fact, the architecture allows for the light to effectively propagate and interfere in multiple optical cavities, formed between the MZI arms and the feedback delay line. The phase shifting element, being the only active element in the reservoir layer, allows the effective modulation of the amount of optical power coupled into the spiral waveguide, whereas the remaining portion is routed to the photodetector.
If we consider the input optical field E_{in} to the first coupler, we can describe the fields at the top (E_1) and bottom (E_2) arms of the asymmetric MZI, after propagating through the respective waveguide lengths, as such:

$$E_1 = \sqrt{\alpha_c \alpha_{wg_1}} \kappa E_{in} \exp(i\beta L_1) \exp(i\frac{\pi}{2}) \tag{4}$$

$$E_2 = \sqrt{\alpha_c \alpha_{wg_2}} t E_{in} \exp(i\beta L_2) \exp(i\Phi) \tag{5}$$

where α_c is the coupler insertion loss (considered equal for simplicity for both ports), $\alpha_{wg} = 10^{-AL/10}$ is the overall waveguide propagation loss for a loss factor A [dB/m] and waveguide length L, κ and t are the cross and through field coupling coefficients, respectively, $\beta = 2\pi n_{eff}/\lambda$ [m^{-1}] is the propagation constant, L_1 and L_2 are the upper and bottom arm lengths [m], respectively, and Φ [rad] is the applied phase shift on the bottom arm. Next, the field E_{out} at the output upper port (that goes into the spiral) and the MZI cross coupling power coefficient can be described as:

$$E_{out} = \sqrt{\alpha_c}(tE_1 + \kappa E_2 \exp(i\frac{\pi}{2})) \tag{6}$$

$$\kappa^2_{_{MZI}} = \left|\frac{E_{out}}{E_{in}}\right|^2 = \alpha_c^2 t^2 \kappa^2 \left[\left|\sqrt{\alpha_{wg_1}} \exp(i\beta L_1) + \sqrt{\alpha_{wg_2}} \exp(i\beta L_2 + \Phi)\right|^2\right] \tag{7}$$

Therefore, $\kappa^2_{_{MZI}}$ is a function of Φ, and consequently, the amount of power going into the spiral waveguide can be controlled by varying Φ. The remaining power goes to the photodetector, constituting the read-out signal that would be sampled. It is worth noting that this is a linear reservoir, even though the photodetector output is proportional to the square of the output field at the readout layer, due to the absence of nonlinearities inside the reservoir layer. Nonetheless, it has been shown before that linear reservoirs can perform just as well as nonlinear reservoirs for certain

tasks [16]. Furthermore, the characteristic timescale of the system is governed only by the photon lifetime inside the cavity, which allows the 'forward' coupling of the virtual node states.

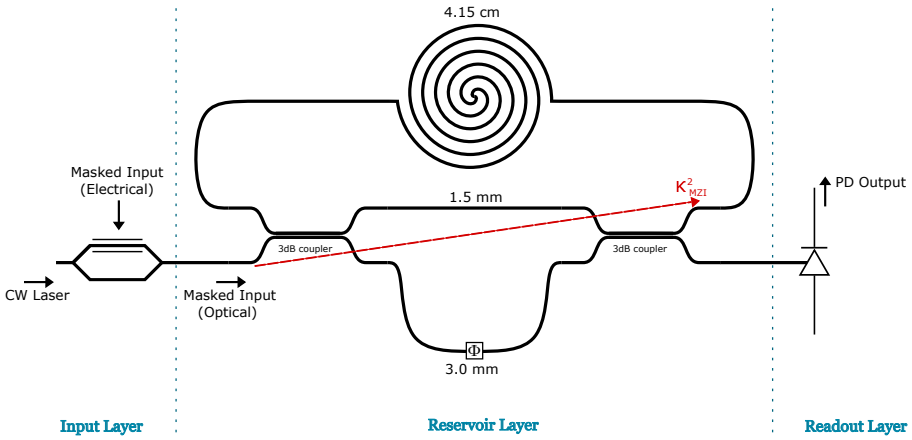

Fig. 2: Proposed architecture: a CW laser is modulated by the electrical input using a Mach-Zender modulator, the reservoir layer consists of the asymmetric MZI connected onto itself with a spiral waveguide, and the readout is performed by a photodetector.

3 Methodology

The inputs of the various tasks are constructed and fed to the circuit, its response is recorded and then trained with linear regression. The 3dB directional couplers are modeled as point couplers, such that there are no additional lengths to be taken into account. All the simulations were carried out with an open source photonic circuit solver [17]. In this study, we consider the operation of the phase shifting element up to V_π, i.e., from 0 to π phase shift, and divide the interval into 101 points, constituting our applied phase values, to get an accurate view of the trend between the trained readout results and the applied phase. The losses assumed were for a lithium niobate on insulator (LNOI) PIC platform [18, 19, 20] The simulation parameters are given in Tab. 1.

Parameter	Value
B	1 Gbit/s
f_s	5-50 GHz
N_v	f_s/B
λ_0	1550.94 nm
n_{eff}	2.2111
n_g	2.2637
α_c	96.6%
A	20 dB/m
P_{in}	10 mW

Table 1: Simulation parameters: B and R_s are the bit rate and sampling frequency, respectively. N_v is the number of virtual nodes, λ_0 is the operation wavelength, n_{eff} and n_g are the effective and group indices for the waveguide, α_c is the directional coupler loss, A is the waveguide propagation loss, and P_{in} is the input optical power.

For both tasks a random mask was applied at the input layer, with N values drawn from a uniform distribution on the interval (0,1], corresponding to the number of nodes N_v in the reservoir. Thus, it operates on the timescale of the nodes, and repeats for every input bit/sample. In this way each mask value can be viewed as the input weight corresponding to the N^{th} reservoir node. Furthermore, the trained output responses were checked against a validation

set to ensure the absence of overfitting.

The size of the reservoir is an important parameter to consider for accurate recall of and up to specific bits into the past. Furthermore, the input power into the reservoir plays a vital role, since the system is eventually limited at the output layer by the noise floor of the photodetector. The photodetector noise is modeled as Gaussian noise with variance corresponding to the different contributions to noise. This noise was then added to the reservoir's output response before the training phase. The integrated photodetector parameters considered are listed in Tab. 2.

Parameter	Value
r	0.7
R_l	100 Ω
NEP_{TIA}	24 $pW/\sqrt{Hz}$
I_d	5 nA

Table 2: Modelled integrated photodetector parameters with responsivity r, load resistance R_l, dark current I_d, and NEP_{TIA} is the noise equivalent power of the transimpedence amplifier.

3.1 Specific Memory Capacity

We first demonstrate the variable memory capacity by varying the phase shift on one arm of the MZI, and thus varying the phase difference between both arms. A training sequence of 500 samples was drawn from an i.i.d. The target sequence is a k-bits delayed copy of the input, testing the reservoir's ability to faithfully reconstruct the input sequence after k bits of delay. The total memory capacity can be varied through changing the phase difference between the MZI arms. More interestingly, however, is that optimal performance of a specific memory capacity MC_k can be optimized as well. Therefore, the reservoir is trained to consider the result for each individual MC_k, instead of the total sum. In addition, the performance for various reservoir sizes was also investigated.

3.2 Temporal bitwise XOR

The bitwise XOR task is a commonly used nontrivial, nonlinear binary task for evaluating a reservoir's performance which was first introduced in [21]. For this task, a pseudo-random bit stream of 3200 bits was generated and fed to the reservoir. The target bit streams were constructed by applying the XOR operation on the bit stream and a k time steps shifted version of it, yielding $x[n] \oplus x[n-k]$, where $x[n]$ is the current input bit. Thus different targets were constructed depending on which bit in the past the XOR operation had to be performed on with the current bit.

To exhaustively explore the entire design space is beyond the scope of this work. However, effects on the reservoir performance of multiple parameters are discussed in section 4, including the effects of input optical power and the size of the reservoir (number of nodes).

3.3 Correlation

We then aim to investigate the correlation between those two above-mentioned tasks (subsections 3.1 and 3.2) and in turn proving the relevance of optimizing the linear memory capacity for memory-specific tasks in reservoir computing. Instead of the BER, we evaluated the performance on the XOR task with the same metric used for the linear memory capacity task (i.e. $1 - NMSE$). Then, the Pearson Correlation Coefficient for the results of both tasks under varying applied phase shift for each k was calculated.

4 Results and Discussion

4.1 Specific Memory Capacity

The results for different k time steps shifts in Fig. 3 show the variation of each MC_k with respect to applied phase shift, and an overall improving behavior as the reservoir size increases.

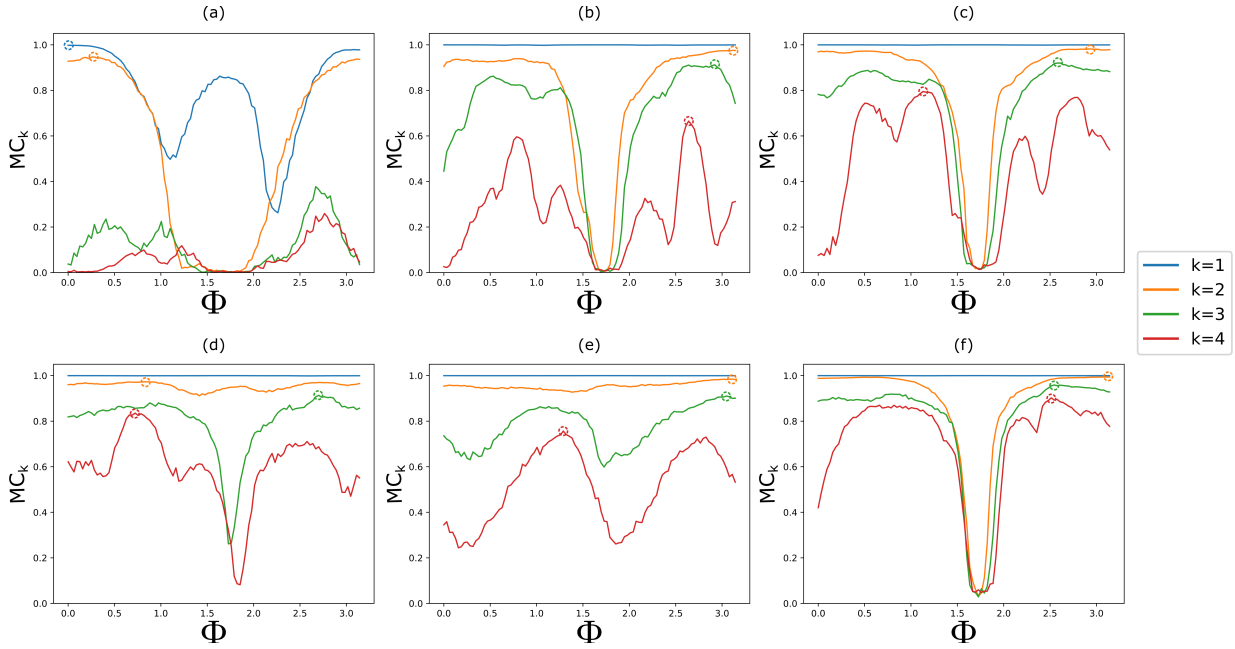

Fig. 3: Performance of the reservoir on solving the linear memory capacity task for different values of applied phase shift Φ [rad] on the MZI arm for different reservoir sizes: (a) N_v=5 (b) N_v=10, (c) N_v=20, (d) N_v=30, (e) N_v=40, (f) N_v=50.

Upon closer examination, one can observe that for several cases the optimal MC_k value for each k occurs at different values of applied phase shift Φ, as shown in circle markers. For example, in Fig. 3(b), while the optimum values for $k = 1$ and $k = 2$ occur similarly at around $\Phi \approx \pi$, for $k = 3$ and $k = 4$ they occur around $\Phi \approx 0.75$ and $\Phi \approx 1.25$, respectively. This necessitates the optimization for each individual k. As the reservoir size increases, a more homogeneous trend for the various MC_k values arises, enabling one to optimize for all k's at a single value of applied phase shift (Fig. 3 (f)). The fact that the memory capacity can be varied to optimally recall k bits into the past can prove useful for other tasks, such as the temporal bitwise XOR task.

4.2 Temporal bitwise XOR

The input bitstream used for training consists of 3200 bits, thus the resolution of the BER is limited to 3.125×10^{-4}. Thus a BER below 10^{-3} is considered as acceptable, as shown in purple in Fig. 4, where results are shown for $k = 1$ to $k = 4$ for various reservoir sizes.

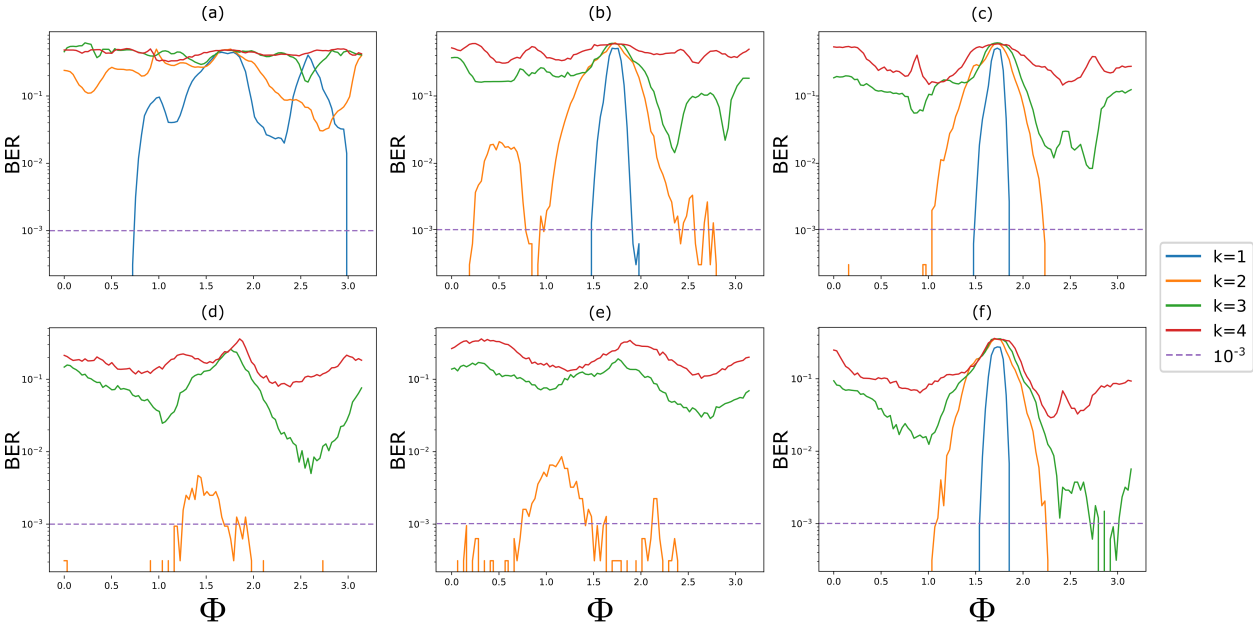

Fig. 4: Performance of the reservoir on solving the temporal bitwise XOR task for different values of applied phase shift Φ [rad] on the MZI arm for different reservoir sizes: (a) 5 Nodes, (b) 10 Nodes, (c) 20 Nodes, (d) 30 Nodes, (e) 40 Nodes, (f) 50 Nodes. Where the blue line is not visible, it is due to BER = 0 everywhere on the plot.

Similar to the memory capacity results, the performance on the XOR task mostly improves as the reservoir size scales. It is shown in Fig. 4(a) that it is possible to do the one bit XOR with 5 nodes, and possibly even less. Furthermore, the input power into the reservoir layer (i.e. after the input modulator) is also considered for three cases, the first case studies the minimum power requirements to do the one bit XOR task successfully (around 500 µW), while the other two cases consider an input power of 20 mW with 20 nodes and 50 nodes, respectively. These two sizes were chosen as they both enable the XOR operation with $k = 3$, however the 50 nodes reservoir shows significantly more reliable performance.

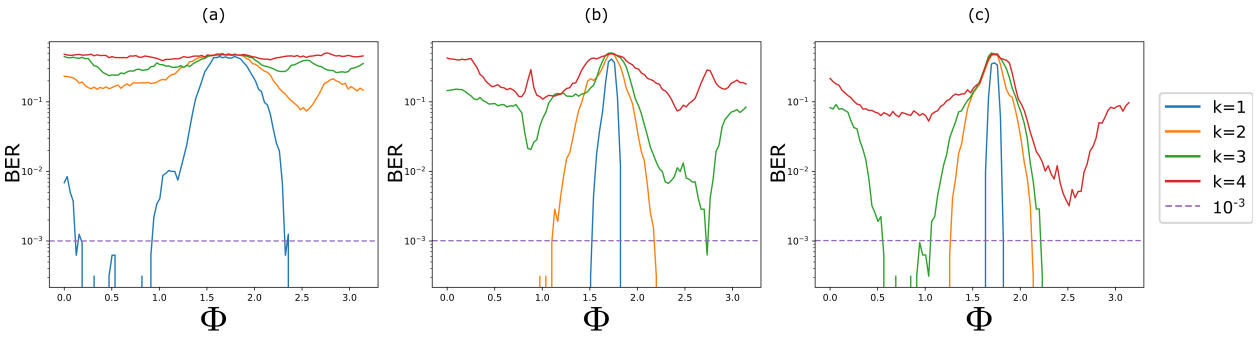

Fig. 5: Three cases for different input powers: (a) 500 µW with 10 nodes , (b) 20 mW with 20 nodes, (c) 20 mW with 50 nodes.

4.3 Correlation

The results in Fig. 6 show a mostly strong correlation for smaller values of k (except $k = 1$), while the correlation strength for more distant values of k increase only for reservoirs with a larger N_v.

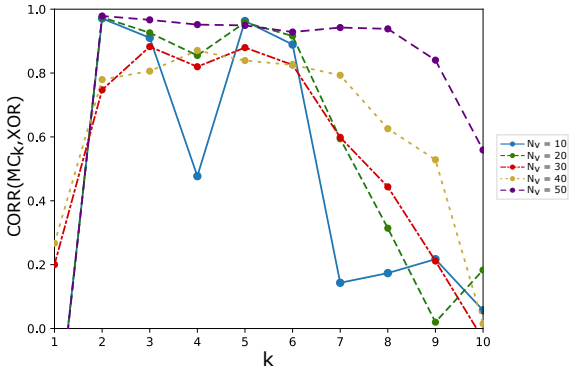

Fig. 6: Correlation between the reservoir's performance on memory capacity and bitwise XOR tasks.

Since the performance for MC_1 with respect to changing the applied phase (Fig. 3) exhibits small deviations (and also for $[n] \oplus [n-1]$ in Fig. 4(d,e)), it is difficult to establish a correlation between them, which is the reason behind the consistently weak correlation values for the first k. Otherwise, the fact that the correlation exists enables one to also predict the reservoir's performance on one task by training it on another, provided they share similar attributes to the tasks presented here.

5 Conclusion

We have proposed a novel photonic architecture for reservoir computing which enables the tuning of the memory capacity in an energy-efficient manner, as the optical power is either in the reservoir or re-routed to the photodetector. This approach provides better performance in terms of power consumption over the more common implementation utilizing an optical attenuator block in the feedback loop where the light is simply coupled out of the system. We have shown results for the linear memory capacity and for the temporal bitwise XOR task. To the best of our knowledge, this is the first time that the individual components of the total linear memory capacity were investigated. Furthermore, the verified correlation between the performance on both tasks justifies the need for optimizing the reservoir's memory for memory-specific tasks, and also opens up the possibility of evaluating a reservoir's performance on one task (or possibly a class of such tasks) by training it on another.

It is also worth mentioning that the proposed reservoir architecture was capable of solving the 10^{th} order nonlinear autoregressive moving average (NARMA 10) task with an NMSE of 0.13 for a reservoir size of 50 nodes. However, when taking into account the noise at the readout layer, it is essential to consider a photodetector with high enough sensitivity and/or averaging, in large part due to the combination of the analog nature of the input stream of the NARMA 10 task and the large memory requirement (up to 10 inputs into the past).

The architecture presented here was not fully optimized for the aforementioned tasks, in part due to the large parameter space. It is therefore possible to obtain even better performance when optimizing, for example, the MZI arm lengths and/or the spiral length.

Declaration of Competing Interest

The authors declare that they have no known competing financial interests or personal relationships that could have appeared to influence the work reported in this paper.

Acknowledgements

This work was supported by the ECLAUSion project which has received funding from the European Union's Horizon 2020 research and innovation program under the Marie Skłodowska-Curie grant agreement No 801512. We acknowledge the support of the International Associated Laboratory in Photonics between France and Australia (LIA ALPhFA). This work was also carried out within the framework of the PHASEPUF project supported by the French "Agence Nationale de la Recherche" under project number ANR-20-CE39-0004.

References

[1] Herbert Jaeger. The" echo state" approach to analysing and training recurrent neural networks-with an erratum note'. *Bonn, Germany: German National Research Center for Information Technology GMD Technical Report*, 148, 01 2001.

[2] *The "Liquid Computer": A Novel Strategy for Real-Time Computing on Time Series*, 2002.

[3] Gouhei Tanaka, Toshiyuki Yamane, Jean Benoit Héroux, Ryosho Nakane, Naoki Kanazawa, Seiji Takeda, Hidetoshi Numata, Daiju Nakano, and Akira Hirose. Recent advances in physical reservoir computing: A review. *Neural Networks*, 115:100–123, 7 2019.

[4] Y. Paquot, F. Duport, A. Smerieri, J. Dambre, B. Schrauwen, M. Haelterman, and S. Massar. Optoelectronic reservoir computing. *Scientific Reports*, 2, 2012.

[5] Quentin Vinckier, François Duport, Anteo Smerieri, Kristof Vandoorne, Peter Bienstman, Marc Haelterman, and Serge Massar. High-performance photonic reservoir computer based on a coherently driven passive cavity. *Optica*, 2(5):438–446, May 2015.

[6] Laurent Larger, Antonio Baylón-Fuentes, Romain Martinenghi, Vladimir S. Udaltsov, Yanne K. Chembo, and Maxime Jacquot. High-speed photonic reservoir computing using a time-delay-based architecture: Million words per second classification. *Physical Review X*, 7, 2 2017.

[7] Kristof Vandoorne, Pauline Mechet, Thomas Van Vaerenbergh, Martin Fiers, Geert Morthier, David Verstraeten, Benjamin Schrauwen, Joni Dambre, and Peter Bienstman. Experimental demonstration of reservoir computing on a silicon photonics chip. *Nature Communications*, 5, 3 2014.

[8] Chihiro Sugano, Kazutaka Kanno, and Atsushi Uchida. Reservoir computing using multiple lasers with feedback on a photonic integrated circuit. *IEEE Journal of Selected Topics in Quantum Electronics*, PP:1–1, 07 2019.

[9] Giovanni Donati, Claudio R. Mirasso, Mattia Mancinelli, Lorenzo Pavesi, and Apostolos Argyris. Microring resonators with external optical feedback for time delay reservoir computing. *Optics Express*, 30:522, 1 2022.

[10] L. Appeltant, M. C. Soriano, G. Van der Sande, J. Danckaert, S. Massar, J. Dambre, B. Schrauwen, C. R. Mirasso, and I. Fischer. Information processing using a single dynamical node as complex system. *Nature Communications*, 2(1):468, Sep 2011.

[11] Herbert Jaeger. Tutorial on training recurrent neural networks, covering bppt, rtrl, ekf and the" echo state network" approach, 2002.

[12] Igor Farkaš and Peter Gergeľ. Maximizing memory capacity of echo state networks with orthogonalized reservoirs. In *2017 International Joint Conference on Neural Networks (IJCNN)*, pages 2437–2442, 2017.

[13] Peter Barančok and Igor Farkaš. Memory capacity of input-driven echo state networks at the edge of chaos. In Stefan Wermter, Cornelius Weber, Włodzisław Duch, Timo Honkela, Petia Koprinkova-Hristova, Sven Magg, Günther Palm, and Alessandro E. P. Villa, editors, *Artificial Neural Networks and Machine Learning – ICANN 2014*, pages 41–48, Cham, 2014. Springer International Publishing.

[14] Xinyu Han, Yi Zhao, and Michael Small. Revisiting the memory capacity in reservoir computing of directed acyclic network. *Chaos: An Interdisciplinary Journal of Nonlinear Science*, 31(3):033106, 2021.

[15] W. D. Sacher, W. M. J. Green, S. Assefa, T. Barwicz, H. Pan, S. M. Shank, Y. A. Vlasov, and J. K. S. Poon. Coupling modulation of microrings at rates beyond the linewidth limit. *Opt. Express*, 21(8):9722–9733, Apr 2013.

[16] Ali Rodan and Peter Tiňo. Minimum complexity echo state network. *IEEE Transactions on Neural Networks*, 22:131–144, 1 2011.

[17] Floris Laporte, Joni Dambre, and Peter Bienstman. Highly parallel simulation and optimization of photonic circuits in time and frequency domain based on the deep-learning framework pytorch. *Scientific Reports*, 9, 12 2019.

[18] Andreas Boes, Bill Corcoran, Lin Chang, John Bowers, and Arnan Mitchell. Status and potential of lithium niobate on insulator (lnoi) for photonic integrated circuits. *Laser and Photonics Reviews*, 12, 4 2018.

[19] Xu Han, Li Chen, Yongheng Jiang, Andreas Frigg, Huifu Xiao, Thach Giang Nguyen, Andreas Boes, Jianhong Yang, Guanghui Ren, Yikai Su, Arnan Mitchell, and Yonghui Tian. Integrated subwavelength gratings on a lithium niobate on insulator platform for mode and polarization manipulation. *Laser & Photonics Reviews*, n/a(n/a):2200130, 2022.

[20] Xu Han, Yongheng Jiang, Andreas Frigg, Huifu Xiao, Pu Zhang, Thach Giang Nguyen, Andreas Boes, Jianhong Yang, Guanghui Ren, Yikai Su, Arnan Mitchell, and Yonghui Tian. Mode and polarization-division multiplexing based on silicon nitride loaded lithium niobate on insulator platform (laser photonics rev. 16(1)/2022). *Laser & Photonics Reviews*, 16(1):2270001, 2022.

[21] Nils Bertschinger and Thomas Natschläger. Real-Time Computation at the Edge of Chaos in Recurrent Neural Networks. *Neural Computation*, 16(7):1413–1436, 07 2004.